AC electrified jets in a flow-focusing device: Jet length scaling

Elena Castro-Hernández,[1,a)] Pablo García-Sánchez,[2] Javier Alzaga-Gimeno,[1] Say Hwa Tan,[3] Jean-Christophe Baret,[4] and Antonio Ramos[2,b)]

[1]*Área de Mecánica de Fluidos, Departamento de Ingeniería Aeroespacial y Mecánica de Fluidos, Universidad de Sevilla, Avenida de los Descubrimientos s/n, 41092 Sevilla, Spain*
[2]*Departamento de Electrónica y Electromagnetismo, Facultad de Física, Universidad de Sevilla, Avenida de Reina Mercedes s/n, 41012 Sevilla, Spain*
[3]*Queensland Micro- and Nanotechnology Centre, Griffith University, Brisbane QLD 4111, Australia*
[4]*CNRS, Univ. Bordeaux, CRPP, UPR 8641, Soft Micro Systems, 115 Avenue Schweitzer, 33600 Pessac, France and Max-Planck Institute for Dynamics and Self-Organization, Droplets, Membranes and Interfaces, Am Fassberg 17, DE-37077 Goettingen, Germany*

(Received 31 March 2016; accepted 4 June 2016; published online 15 June 2016)

We use a microfluidic flow-focusing device with integrated electrodes for controlling the production of water-in-oil drops. In a previous work, we reported that very long jets can be formed upon application of AC fields. We now study in detail the appearance of the long jets as a function of the electrical parameters, i.e., water conductivity, signal frequency, and voltage amplitude. For intermediate frequencies, we find a threshold voltage above which the jet length rapidly increases. Interestingly, this abrupt transition vanishes for high frequencies of the signal and the jet length grows smoothly with voltage. For frequencies below a threshold value, we previously reported a transition from a well-behaved uniform jet to highly unstable liquid structures in which axisymmetry is lost rather abruptly. These liquid filaments eventually break into droplets of different sizes. In this work, we characterize this transition with a diagram as a function of voltage and liquid conductivity. The electrical response of the long jets was studied via a distributed element circuit model. The model allows us to estimate the electric potential at the tip of the jet revealing that, for any combination of the electrical parameters, the breakup of the jet occurs at a critical value of this potential. We show that this voltage is around 550 V for our device geometry and choice of flow rates. *Published by AIP Publishing*. [http://dx.doi.org/10.1063/1.4954194]

I. INTRODUCTION

Microfluidics provides new means to study the rheology of complex fluids.[1] The fine control of channel geometry provided by microfabrication techniques and replica molding[2] is especially appealing to investigate the flow patterns in multiphase systems, a problem of relevance to understand emulsification and foaming. In addition to the fundamental questions related to flows and instabilities in multiphase systems, the recent use of microfluidics in practical applications[3] is a further motivation to investigate these flow patterns. In the classical problem of the dripping to jetting transition at a microfluidic junction, the theoretical background to understand a liquid jet stability in coflowing fluids involves the description of both, the absolute and convective instabilities along the jet.[4,5] In an absolute instability, perturbations grow from a fixed point in space. The disturbances grow and propagate in both, the downstream and

[a)]elenacastro@us.es
[b)]ramos@us.es

upstream directions. On the other hand, the perturbations in a convective instability propagate downstream as they grow, which allows a long and continuous fluid thread to persist consistently. Nevertheless, long jets are not always a result of a convective instability, as it was shown by Utada *et al.*[5] At the microscale, microfluidic devices provide the necessary conditions which favour controllable thread length production with extremely high accuracy and precision. Well defined and controllable jets could then be interesting for applications in the field of material science and fibre synthesis.[6]

In the context of applications, actively controlling such a transition is of interest to design switchable microsystems. Recently, Tan *et al.*[7] designed an electrocapillary system usable to control the dripping to jetting transition, for fixed flow conditions. It was shown that an AC electric field can be applied into a microfluidic flow focusing device to provide an additional dimensional control in the production of water droplets in oil. This method of actuation is a viable tool to modulate both, the droplet size at the nozzle in the dripping regime and the thread length in the jetting regime. The electric field induces the transition of droplet production from the dripping to the jetting regime as the electric field intensity increases. This method of electroactuation is sufficiently fast to switch reliably between droplet sizes (or frequency production[8]). These electro-flow focusing devices have been successfully used[9] in order to produce long jets that cannot be obtained by other means under the same flow conditions.

In our previous work, we found that for a constant voltage amplitude of 1000 V peak-to-peak, the jet length was proportional to the square root of the conductivity to frequency ratio. In order to clarify the physical mechanisms that produce these long jets, we have performed a thoroughly experimental characterization of the applied voltage effect on the jet length. In particular, for intermediate values of the frequency, we find long jets beyond a threshold voltage. However, for high frequencies the jet length increases smoothly. When the signal frequency is below a critical value ($f \leq f_{\mathrm{mess}}$), there is a transition between the axisymmetric jet and an unstable droplet generation regime.[7,9] We report a stability map displaying these critical values, for different voltages and conductivities. In Sec. IV, we make use of a distributed element circuit model to describe the decay of the voltage difference between a long jet and the downstream electrodes.[9] We apply this model to calculate the voltage at the tip for all long jets. In all cases, we find that the voltage at the tip of the jet is around 550 V peak-to-peak, irrespective of the applied voltage, signal frequency, and/or jet conductivity. This result indicates that the breakup takes place for a given solution of the electric field around the tip.

II. EXPERIMENTAL SETUP

Soft lithography techniques are used to assemble a microfluidic electro-flow focusing device by replica molding in polydimethylsiloxane (PDMS, Dow Corning, relative permittivity $\varepsilon_{r,\mathrm{PDMS}} = 2.5$). Figure 1 shows a schematic view of the device with a cross-junction $w = 100\,\mu$m wide and $h = 35\,\mu$m tall. Two sets of electrodes, with the same width and height, are patterned on both sides on the junction running parallel to the inner inlet and outlet channels and they are produced using the microsolidics technique.[7,10] The distance between the electrodes and the microfluidic channel is $d_e = 35\,\mu$m. The length of the upstream electrodes is $l_e = 2.2$ mm. The PDMS device is plasma bonded to the non-conductive side of an Indium Tin Oxide glass (ITO, thickness 1 mm, $\varepsilon_{r,\mathrm{glass}} = 7.5$). The conductive side of the ITO glass is used as a counter electrode.

A water-in-oil (W/O) emulsion is produced by focusing an inner aqueous stream (dispersed phase) with two outer oil streams (continuous phase). The inner and outer flow rates, Q_i and Q_o, respectively, are controlled by means of a double syringe pump (model 33, Harvard Apparatus). The dispersed phase is an aqueous solution of KCl in Milli-Q water with a viscosity $\eta_i = 1$ cP and an electrical conductivity varying between $\kappa = 3 \times 10^{-4}$ S/m and $\kappa = 3 \times 10^{-2}$ S/m. The continuous phase is mineral oil (RTM14, Sigma Aldrich) with a viscosity of $\eta_o = 100$ cP. The relative permittivity of mineral oil is $\varepsilon_{r,o} = 2.1$, and its electrical conductivity is negligible ($\kappa_o < 10^{-10}$ S/m), being considered from now on as a perfect insulator. A 5 % (w/w) of a non-ionic surfactant (Span 80, Sigma Aldrich) is added to the continuous

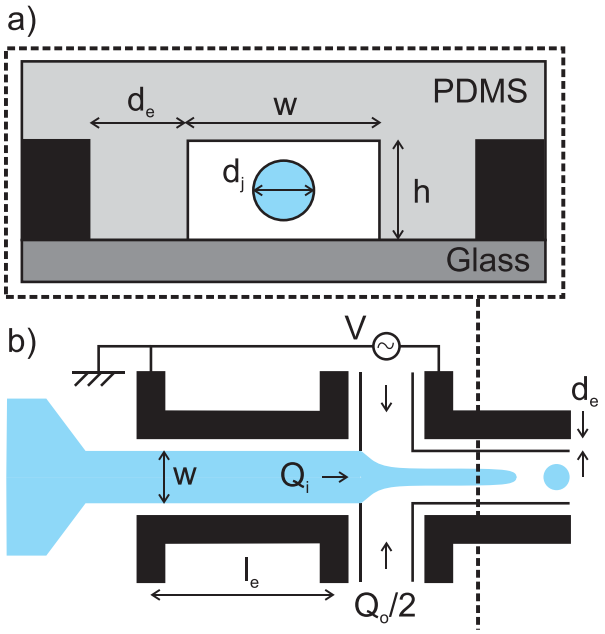

FIG. 1. (a) Cross section of the device at the level of the outlet microchannel. (b) Sketch of a microfluidic flow focusing device under an AC electric field. The electrodes are in black and the dispersed phase in blue.

phase lowering the surface tension of the liquid to liquid interface from $\sigma = 40\,\mathrm{mN/m}$ to $\sigma = 5\,\mathrm{mN/m}$, being this value independent of the KCl concentration.

The high-voltage is applied to the downstream pair of electrodes while the others are grounded, which guarantees that the incoming liquid has zero potential.[9] As a consequence, there is an applied AC potential difference between the inner liquid emerging from the upstream electrodes and the downstream electrodes. A sinusoidal voltage with frequencies varying from $f = 1\,\mathrm{kHz}$ to $f = 50\,\mathrm{kHz}$ (TGA1244, TTi) is amplified from $V_{pp} = 0\,\mathrm{V}$ to $V_{pp} = 1000\,\mathrm{V}$ (PZD700A, Trek). The microfluidic device is placed on an inverted microscope (Eclipse Ti-U, Nikon) connected to a high-speed camera (Phantom v7.3) with a resolution of $800 \times 256\,\mathrm{px}^2$ when operated at an acquisition rate of 10^4 fps. The jet diameter, d_j, and jet length, l_j, of at least 100 images are measured via image processing (Matlab, Mathworks, and ImageJ).

III. EXPERIMENTAL RESULTS

Long jets can be produced by means of hydrodynamic forces exclusively. In general, for low values of the flow rates, the dripping regime is observed and the production of monodisperse droplets takes place in a region close to the junction. A jetting regime is reported for large flow rates. In this situation, if the outer viscous stresses on the jet interface are of the order of the surface tension confinement forces, a slender jet appears which eventually breaks up into uniform droplets.[5,11–15]

Liu *et al.*[16] applied DC electric fields to control the droplet production in a flow focusing device. They observed very long jets for high applied voltages and a suitable flow rate ratio between the two phases. As we previously reported,[9] the simple use of an AC voltage elongates the jet and allows for a precise control of the breakup length, which might provide an alternative technique to produce fibers-like shape structures.[6] In order to study these long jets, we perform experiments with an outer fluid viscosity $\eta_o = 100\,\mathrm{cP}$ and an inner to outer flow rate ratio $Q_i/Q_o = 0.125$ ($Q_i = 50\,\mu\mathrm{l/h}$, $Q_o = 400\,\mu\mathrm{l/h}$). In this situation, jetting takes place even in the absence of electric field although with smaller jet lengths (Figures 2(a) and 4(a)). For these flow rates, the jet issues around 500 droplets per second. We carry out series of experiments varying the inner conductivities ($\kappa = 3 \times 10^{-4}$, 1×10^{-3}, 3×10^{-3}, 1×10^{-2}, and $3 \times 10^{-2}\,\mathrm{S/m}$), the frequency ($f = 0-50\,\mathrm{kHz}$) and the voltage ($V_{pp} = 0-1000\,\mathrm{V}$) of the applied AC field.

Figure 2 shows the effect of increasing the voltage amplitude on the jet length for a given water conductivity ($\kappa = 3 \times 10^{-3}$ S/m) and signal frequency ($f = 9$ kHz). Increasing the voltage results in longer jets, and a jet of 650 μm in length is obtained when the maximum voltage supplied by the amplifier is applied (1000 V). The same trend is found for all the tested water conductivities obtaining longer jets for higher values of the conductivity.

Figure 3 displays measurements of the jet length versus the applied voltage for a given conductivity ($\kappa = 3 \times 10^{-3}$ S/m) and different frequencies. The jet length is measured from the beginning of the downstream electrodes. These measurements are an average of 100 ruptures, and the dispersion is approximately given by the jet diameter, about 10 μm. For low frequencies ($f \leq 9$ kHz), it also shows an abrupt change in jet length as voltage increases. This threshold voltage is around $V_{pp} \simeq 600$ V. The inset shows a more detailed study for $f = 5$ kHz where the voltage was increased from 500 V to 600 and decreased back to 500 V. Decreasing the voltage the change in jet length is smooth and, as a result, a hysteresis curve is obtained. Interestingly, this abrupt transition vanishes for high frequencies of the signal; the jet length grows smoothly with voltage and the hysteresis disappears. We have observed the same hysteretic behavior for all water conductivities. In particular for high conductivities ($\kappa = 10$ and 30 mS/m), the transition was abrupt for all tested signal frequencies.

Figure 4 shows the effect of decreasing the signal frequency on the jet length for a given water conductivity ($\kappa = 3 \times 10^{-3}$ S/m) and signal amplitude ($V_{pp} = 1000$ V). For comparison, we show in Figure 4(a), the situation where no voltage is applied. Accordingly to previous results,[9] longer jets are found as the frequency of the signal is reduced (sequence from (b) to (e) in Figure 4) and the rest of the parameters are kept constant. The figure also shows that the *unstable* regime takes place for frequencies low enough ($f \leq f_{\text{mess}}$). The same trend is observed for all water conductivities. For a given voltage and frequency, longer jets are obtained for

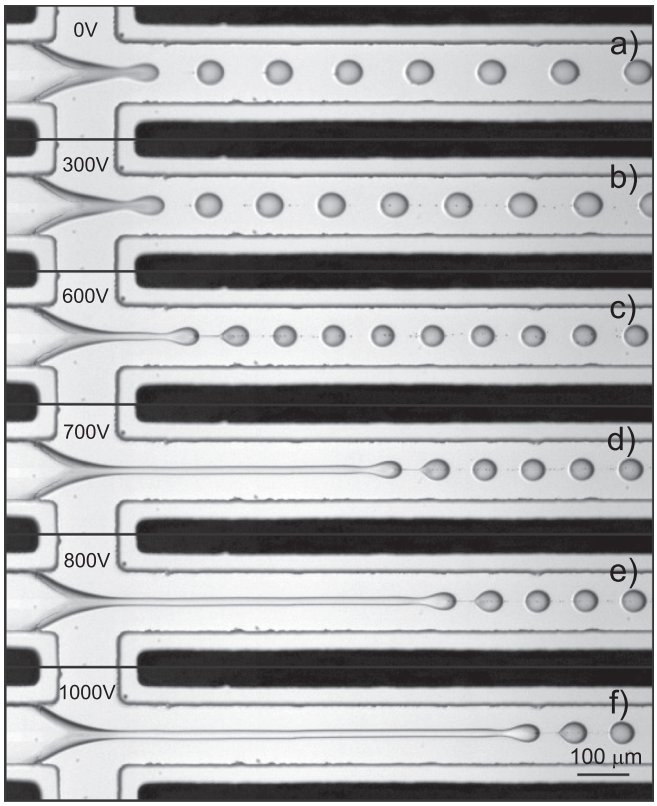

FIG. 2. Series of images showing the effect of increasing the signal voltage on the jet length for $Q_i = 50\,\mu$l/h, $Q_o = 400\,\mu$l/h, $\eta_o = 100$ cP, $\kappa = 3 \times 10^{-3}$ S/m and $f = 9$ kHz: (a) $V_{pp} = 0$ V; (b) $V_{pp} = 300$ V; (c) $V_{pp} = 600$ V; (d) $V_{pp} = 700$ V; (e) $V_{pp} = 800$ V; (f) $V_{pp} = 1000$ V.

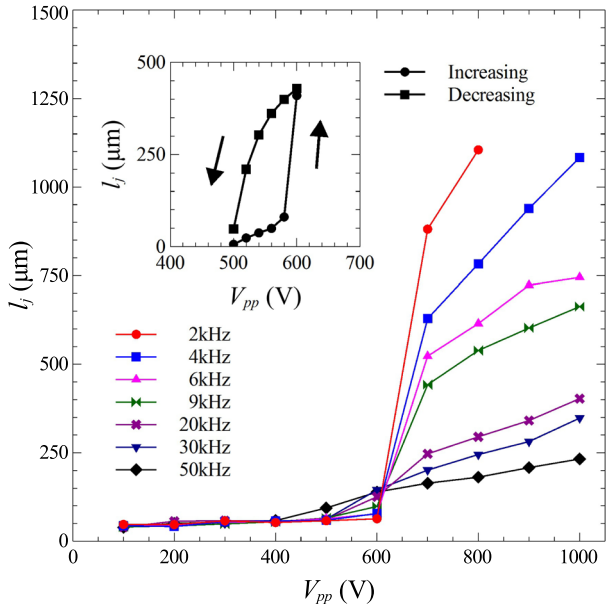

FIG. 3. Jet length versus signal voltage for different values of the signal frequency for $Q_i = 50\,\mu$l/h, $Q_o = 400\,\mu$l/h, $\eta_o = 100$ cP, and $\kappa = 3 \times 10^{-3}$ S/m. The inset shows the hysteresis loop when increasing or decreasing the voltage amplitude for $f = 5$ kHz.

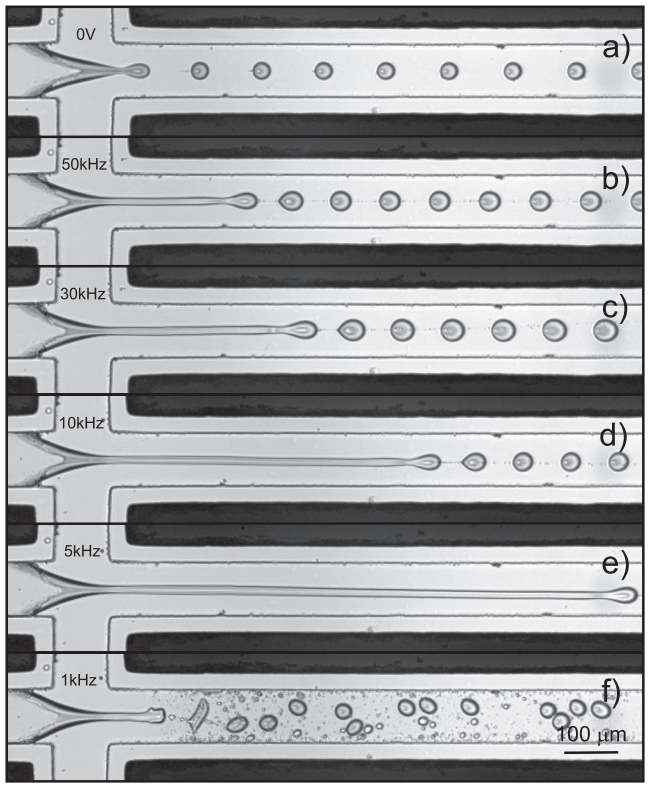

FIG. 4. Series of images showing the effect of decreasing the signal frequency on the jet length for $Q_i = 50\,\mu$l/h, $Q_o = 400\,\mu$l/h, $\eta_o = 100$ cP, $\kappa = 3 \times 10^{-3}$ S/m, and $V_{pp} = 1000$ V: (a) $V_{pp} = 0$ V; (b) $f = 50$ kHz; (c) $f = 30$ kHz; (d) $f = 10$ kHz; (e) $f = 5$ kHz; (f) $f = 1$ kHz.

higher conductivities. The transition frequency to the unstable regime (see Figure 4(f)) depends on both, the water conductivity and the applied voltage amplitude, as it was reported in previous observations by Tan *et al.*[7] In this work, a transition from jetting to unstable drop production was found for a frequency which linearly increases with water conductivity for $\eta_o = 30\,\text{cP}$. When the instability takes place, the jet wets the glass wall and produces liquid filaments that eventually break into droplets of different sizes.

Figure 5 shows f_{mess} for all the tested conductivities and different values of the voltage amplitude. The transition frequency increases with water conductivity while, apparently, below $\kappa = 1\,\text{mS/m}$ is constant. This figure also demonstrates that, for a fixed conductivity, the larger the voltage the larger f_{mess}, i.e., the unstable region increases. Since the jet is attracted to both electrodes, any nonaxisymmetric perturbation can be amplified for high electric field, which could be the reason for this instability. To the best of our knowledge, the onset of this instability below a certain frequency lacks of a theoretical explanation. Castro-Hernández *et al.*[9] showed for a voltage amplitude of 1000 V that the jet length is proportional to $\sqrt{\kappa/f}$. Figure 6 shows the same scaling for each applied voltage for those cases where a long jet is established ($l_j > w$). The figure also shows the best fit curves to a power law for each voltage. All exponents obtained from the fitting are close to $-1/2$. This key clue, provided by the experimental data, will be rationalized by theoretical analysis in Sec. IV.

IV. DISCUSSION

Table I summarizes some relevant dimensionless numbers involved in our experiments. Inner and outer Reynolds numbers are small, implying that inertial effects should be negligible as it is usual in these types of geometries. Here, the average velocity of the dispersed phase was computed as $U_i = 4Q_i/\pi d_j^2$. Electrical forces are characterized by the electrical Bond number B_e, defined as the time-averaged electrical pressure on the interface $\varepsilon_o E_{rms}^2/2$ divided by the capillary pressure σ/ℓ, where ℓ is a typical radius of curvature. For the maximum applied voltage of 1000 V peak to peak, the characteristic electric field in the junction is estimated as $E_{rms} = 3.5 \times 10^6$ V/m. From this value, the electrical Bond number for the cone-jet transition is $B_{e,\text{cone}} \sim 0.5$, taking as typical cone radius of curvature $\ell = 20\,\mu\text{m}$. Since the experimental

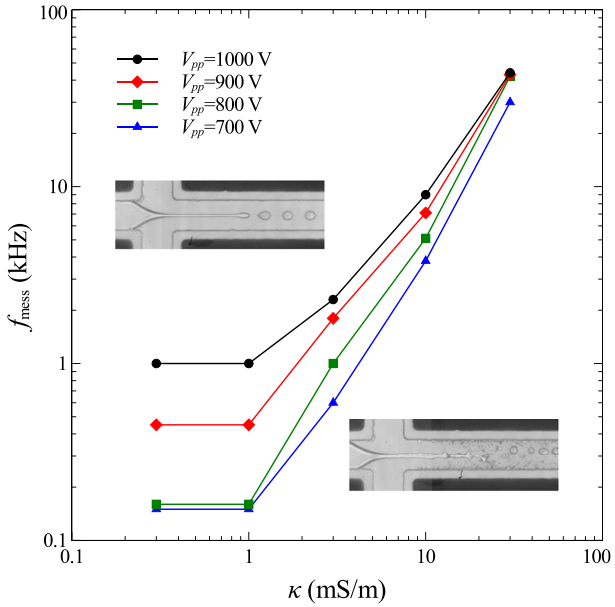

FIG. 5. Transition frequency versus dispersed phase conductivity for different values of the applied voltage for $Q_i = 50\,\mu\text{l/h}$, $Q_o = 400\,\mu\text{l/h}$, and $\eta_o = 100\,\text{cP}$.

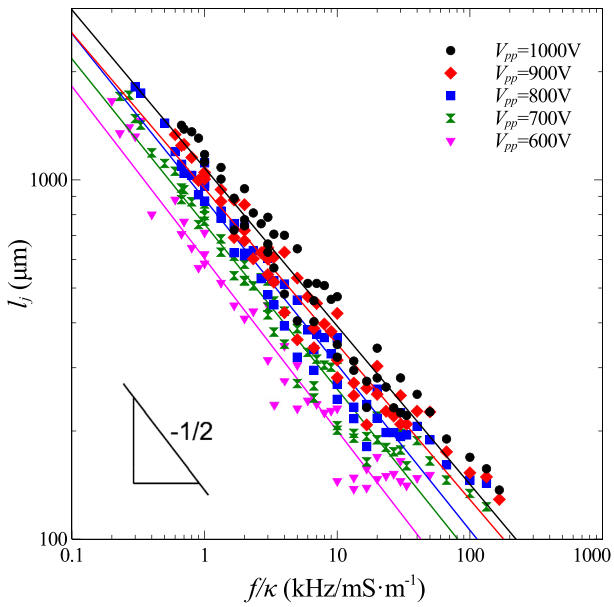

FIG. 6. Jet length versus f/κ for different values of the signal voltage for $Q_i = 50\,\mu$l/h, $Q_o = 400\,\mu$l/h, and $\eta_o = 100$ cP.

radius of the jet is almost constant $d_j/2 = 6.5\,\mu$m and the electric field on the surface of the jet is $E_{rms} = 2.3 \times 10^7$ V/m (computed numerically using finite elements), the electrical Bond number for the jet at the channel entrance is $B_{e,\text{jet}} \sim 6$ for an applied voltage of 1000 V. This indicates that B_e changes by an order of magnitude in the cone-to-jet transition. Inner and outer capillary numbers are below unity, meanwhile the electrical Bond number of the jet is much greater (values between $B_e \sim 2$ for 600 V applied voltage and $B_e \sim 6$ for 1000 V applied voltage), which strengthens the idea that the electric forces are responsible for the formation of such long jets.

The experiments show that the length of the jet increases for increasing applied voltage, decreasing frequency, and increasing water conductivity. When either the applied voltage is small, the frequency is high, or the conductivity is small, there is a very short jet that breaks into drops rapidly. Based upon these experimental facts and the way the electric field amplitude decreases as we move along the jet inside the channel,[9] we hypothesize that the jet breaks into drops when the electric field amplitude around the jet tip is below a certain value. The voltage difference, V, between the jet and the channel electrodes as a function of distance z inside the channel can be studied by using concepts of transmission line (or distributed element) theory.[17] The transmission line model is valid when there is translational symmetry and the characteristic length along the line is much greater than the characteristic length in transverse direction. This methodology was successfully applied by Baret *et al.*[18] to model the electric response of a liquid finger in electrowetting experiments.

Using phasors, the potential drop in the axial direction along a conducting jet is (see Figure 7)

TABLE I. Values of the dimensionless relevant parameters involved in this problem. Electrical Bond number was calculated for $V_{pp} = 1000$ V.

$\eta_i/\eta_o = 0.01$	$Q_i/Q_o = 0.125$
$Re_o = \rho_o U_o h/\eta_o \simeq 0.01$	$Re_i = \rho_i U_i d_j/\eta_i \simeq 0.7$
$Ca_o = \eta_0 U_0/\sigma \simeq 0.5$	$Ca_i = \eta_i U_i/\sigma \simeq 0.02$
$B_{\text{e,cone}} = \varepsilon_o E_{rms}^2 \ell/2\sigma \simeq 0.5$	$B_{\text{e,jet}} = \varepsilon_o E_{rms}^2 d_j/4\sigma \simeq 6$

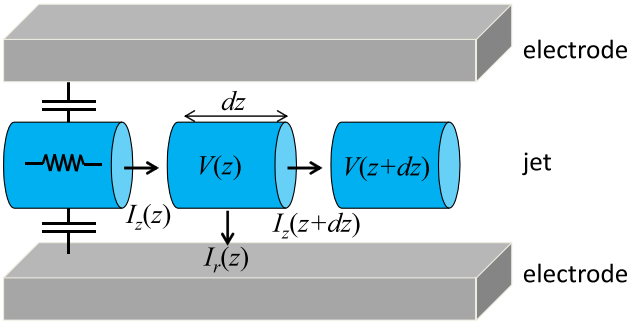

FIG. 7. Sketch of the transmission line model. The resistive jet is coupled capacitively to the electrodes.

$$V(z) - V(z+dz) = \frac{dz}{\kappa\pi a^2} I(z) \Rightarrow -\frac{\partial V}{\partial z} = \frac{I}{\kappa\pi a^2}\,, \tag{1}$$

where $I(z)$ is the current intensity carried by the jet at z, κ is the liquid conductivity, and $a = d_j/2$ is the jet radius. Charge conservation leads to the current intensity at z should be equal to the current at $z + dz$ plus the displacement current leaving the jet interface

$$I(z) = I(z+dz) + i\omega C V(z) \Rightarrow -\frac{\partial I}{\partial z} = i\omega C V\,, \tag{2}$$

where C is the capacitance per unit of length and $i = \sqrt{-1}$ is the imaginary unit. The differential equation that describes the potential is finally

$$\frac{\partial^2 V}{\partial z^2} = \frac{i\omega C}{\kappa\pi a^2} V\,. \tag{3}$$

The boundary conditions are of fixed applied voltage at the entrance, $V(z=0) = V_0$, and negligible electrical current at the jet tip, $I(z = l_j) \approx 0$. For this last boundary condition, we assume that the current transported by the drops issuing from jet tip is negligible (see below). Therefore, according to the transmission line model, the potential along the jet is

$$V(z) = V_0 \frac{\cosh\left[(1+i)(l_j - z)/\delta\right]}{\cosh\left[(1+i)l_j/\delta\right]}, \quad \text{with } \delta = a\sqrt{\frac{2\kappa\pi}{\omega C}}\,. \tag{4}$$

We obtain the capacitance per unit of length C numerically by using the finite element solver COMSOL and taking into account the dimensions of our system in a cross-section (see Figure 1(b)). The numerically obtained value for C is 5.1×10^{-11} F/m. The approximation is valid when the characteristic axial length, δ, is much greater than the characteristic transverse length. The greatest transverse length is the distance between the jet and the electrodes, which is around 75 μm. The values of δ that can be computed from the values of f/κ in Figure 6 are greater or much greater than 75 μm. For instance, for $\kappa = 10^{-3}$ S/m, $a = 6.5\,\mu$m, $f = 5$ kHz, we get $\delta = 410\,\mu$m.

Figure 8 shows jet lengths in units of radius a versus nondimensional frequency $\Omega = \omega C/\kappa$ for an applied voltage of 1000 V and the five water conductivities. The figure also shows the functions δ/a and $2\delta/a$. As can be seen, the jet breaks into drops at a distance from the entrance between δ and 2δ for this applied voltage. Interestingly, δ is proportional to $\sqrt{\kappa/\omega}$, in agreement with the observed trend for jet length of Figure 6.

Figure 9 shows the absolute value of the voltage $|V|$ as a function of z along the jet, as given in Equation (4). We can see that the voltage amplitude is a decreasing function of z. The electrical Bond number, being proportional to V_{rms}^2, is also a decreasing function of z. In our hypothesis, there is a threshold voltage at the tip (or equivalently, a threshold electrical Bond

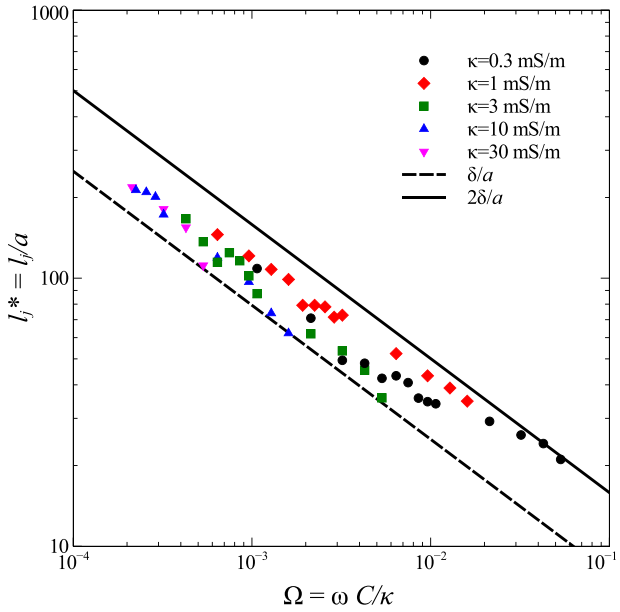

FIG. 8. Dimensionless jet length as a function of nondimensional frequency for different values of the conductivity for $Q_i = 50\,\mu$l/h, $Q_o = 400\,\mu$l/h, $\eta_o = 100$ cP, and $V_{pp} = 1000$ V.

number) below which the jet breaks into drops. Figure 10 plots the average of l_j/δ (jet length in units of δ) and the corresponding standard deviation for each applied voltage. For making this plot we have used the experimental values of Figure 6. For instance, each l_j value corresponding to an applied voltage of 1000 V is divided by its corresponding δ and then averaged. The result is $l_j/\delta \approx 1.4 \pm 0.3$, as can also be extracted from Figure 8 where all jet lengths are between δ and 2δ. The figure also plots three curves of constant voltage at the tip $V(l_j)$. From Equation (4), these curves are given by expression $V(l_j) = V_0/|\cosh[(1+i)l_j/\delta]|$. The voltage at the tip that best fits the experimental points is 550 V peak to peak. This value corresponds to an electrical Bond number $B_e = 1.8$. Therefore, we have obtained a master curve for our experiments that tells us which is the most probable length of breakup for a given applied voltage, signal frequency, and water conductivity. Moreover, the voltage of 550 V is close to the experimental threshold voltage which is observed in Figure 3. This plot confirms our hypothesis that there is a threshold voltage at the tip below which the jet breaks into drops. The fact that the breakup occurs for a given voltage at the tip (550 V peak to peak for our experimental conditions) demands a theoretical explanation.

The model is based upon several approximations that we now justify. The convection of charge by the moving jet interface was neglected in front of the ohmic current through the jet

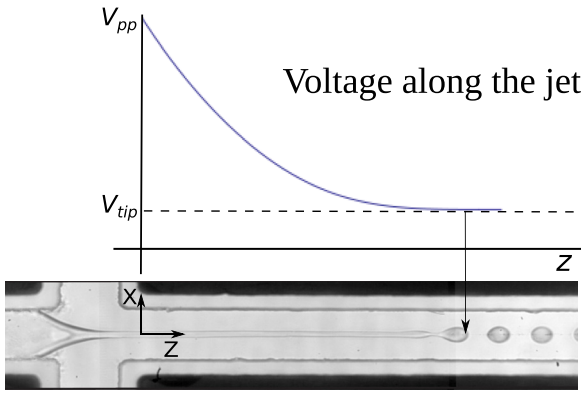

FIG. 9. Voltage amplitude as a function of axial length of the jet.

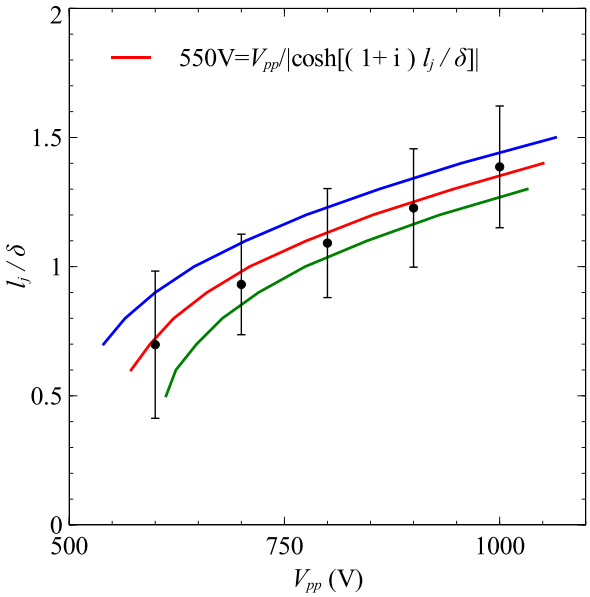

FIG. 10. Jet length in units of δ for each applied voltage. Continuous lines depict curves of equal voltage at the jet tip: red 550 V, blue 600 V, green 500 V.

bulk. The ratio between convection and conduction currents is called the electric Reynolds number.[19] The convection current at a certain axial location is $I_{\text{conv}} = 2\pi a q_s U_i$, where q_s is the induced surface charge on the jet given approximately by $\varepsilon_o E_n$, with E_n being the outer normal electric field. The conduction current through the jet is $I_{\text{ohm}} = \pi a^2 \kappa E_z$ where E_z is the axial electric field. The electric Reynolds number becomes $I_{\text{conv}}/I_{\text{ohm}} \sim \varepsilon_o \delta U_i 2/\kappa a^2$, where we have used that $E_n/E_z \sim \delta/a$ in our model. The higher δ values correspond to the lower frequencies, for $f = 3$ kHz and for the smallest conductivity (0.3 mS/m), the ratio between convected and ohmic currents is of the order of 0.05 and we can safely ignore the motion of the jet when computing the fields. The displacement current inside the jet has also been neglected in front of the ohmic current. This is valid if $\varepsilon_i \omega/\kappa \ll 1$, which is fulfilled for the signal frequencies we are dealing with, $\varepsilon_i \omega/\kappa \sim 4 \times 10^{-3}$ for $f = 1$ kHz, and $\kappa = 10^{-3}$ S/m. Boundary condition $I(l_j) = 0$ assumes that the current transported by the issuing drops is negligible. This current could be either convected charge by the drops or capacitive current through coupling between jet tip and drops. The convected current by the drops should be of the same order as the one convected by the jet, already very small. The capacitive current due to the drops can be compared to the capacitive current leaving the surface of the jet. The ratio between these currents is given by the ratio between capacitances, which is of the order of R/δ (with R being the drop radius) and this number is very small.

V. CONCLUSIONS

Long water jets in a flow focusing device were generated upon application of AC fields. The length of the jet was measured as a function of water conductivity, signal frequency, and voltage amplitude. It was found a threshold voltage above which the jet length increases very fast. The measurements of the length show a hysteresis loop around this threshold voltage. For high frequencies of the AC signal ($f \geq 10$ kHz), the transition to long jets is not abrupt and the hysteresis disappears. The distributed element circuit model of the system provides a way of evaluating the electric potential at the tip of the jet as a function of the electrical parameters. We found that, for all combinations of these parameters at which a long jet is formed, the electric potential at the tip of the jet is around 550 V. This result, together with the similarity of the tip geometry for all long jets, seems to confirm our hypothesis that the jet breakup occurs for a given electric field distribution around the tip. For low frequencies of the AC signals, we

observed the disruption of jet into many small droplets of different sizes. Our measurements show that the lower the liquid conductivity, the lower the frequency signal required for this instability to appear. Also, for increasing applied voltage the instability region increases, i.e., f_{mess} increases. These results point to a critical value of the electric field at the jet surface at which, possibly, a nonaxisymmetric instability leads to the jet disruption.

ACKNOWLEDGMENTS

The authors would like to acknowledge financial support by the ERC (FP7/2007-2013/ERC Grant Agreement No. 306385–SofI), from the Spanish Government Ministry MEC under Contract No. FIS2014-54539-P and Regional Government Junta de Andalucía under Contract No. P11-FQM-7919. They also are grateful to the French State in the frame of the "Investments for the future" Programme IdEx Bordeaux, reference ANR-10-IDEX-03-02. S. H. Tan gratefully acknowledges the support of Griffith University Post doctorate fellowship, New Researcher grant, linkage grant (LP150100153) and Griffith University-Peking University collaboration grant.

[1]K. M. Schultz and E. M. Furst, "High-throughput rheology in a microfluidic device," Lab Chip **11**, 3802 (2011).
[2]Y. Xia and G. M. Whitesides, "Soft lithography," Annu. Rev. Mater. Sci. **28**, 153 (1998).
[3]A. B. Theberge, F. Courtois, Y. Schaerli, M. Fischlechner, C. Abell, F. Hollfelder, and W. T. Huck, "Microdroplets in microfluidics: an evolving platform for discoveries in chemistry and biology," Angew. Chem. Int. Ed. **49**, 5846 (2010).
[4]P. Guillot, A. Colin, A. S. Utada, and A. Ajdari, "Stability of a jet in confined pressure-driven biphasic flows at low Reynolds numbers," Phys. Rev. Lett. **99**(10), 104502 (2007).
[5]A. S. Utada, A. Fernández-Nieves, J. M. Gordillo, and D. Weitz, "Absolute instability of a liquid jet in a coflowing stream," Phys. Rev. Lett. **100**, 014502 (2008).
[6]J. Nunes, S. Tsai, J. Wan, and H. Stone, "Dripping and jetting in microfluidic multiphase flows applied to particle and fibre synthesis," J. Phys. D: Appl. Phys. **46**, 114002 (2013).
[7]S. H. Tan, B. Semin, and J.-C. Baret, "Microfluidic flow-focusing in ac electric fields," Lab Chip **14**, 1099 (2014).
[8]S. H. Tan, F. Maes, B. Semin, J. Vrignon, and J.-C. Baret, "The microfluidic jukebox," Sci. Rep. **4**, 4787 (2014).
[9]E. Castro-Hernández, P. García-Sánchez, S. H. Tan, A. M. Gañán-Calvo, J.-C. Baret, and A. Ramos, "Breakup length of ac electrified jets in a microfluidic flow-focusing junction," Microfluid. Nanofluid. **19**, 787 (2015).
[10]A. C. Siegel, S. S. Shevkoplyas, D. B. Weibel, D. A. Bruzewicz, A. W. Martinez, and G. M. Whitesides, "Cofabrication of electromagnets and microfluidic systems in poly(dimethylsiloxane)," Angew. Chem. **118**, 7031 (2006).
[11]A. M. Gañán-Calvo, R. González-Prieto, P. Riesco-Chueca, M. A. Herrada, and M. Flores-Mosquera, "Focusing capillary jets close to the continuum limit," Nat. Phys. **3**, 737 (2007).
[12]A. M. Gañán-Calvo, "Unconditional jetting," Phys. Rev. E **78**, 026304 (2008).
[13]T. Cubaud and T. G. Mason, "Capillary threads and viscous droplets in square microchannels," Phys. Fluids **20**, 053302 (2008).
[14]M. L. Cordero, F. Gallaire, and C. N. Baroud, "Quantitative analysis of the dripping and jetting regimes in co-flowing capillary jets," Phys. Fluids **23**, 094111 (2011).
[15]E. Castro-Hernández, F. Campo-Cortés, and J. M. Gordillo, "Slender-body theory for the generation of micrometre-sized emulsions through tip streaming," J. Fluid Mech. **698**, 423 (2012).
[16]D. Liu, B. Hakimi, M. Volny, J. Rolfs, R. K. Anand, F. Turecek, and D. T. Chiu, "Modulating patterns of two-phase flow with electric fields," Biomicrofluidics **8**, 044106 (2014).
[17]S. Ramo, J. R. Whinnery, and T. Van Duzer, *Fields and Waves in Communication Electronics* (Wiley, 2008).
[18]J.-C. Baret, M. Decré, S. Herminghaus, and R. Seemann, "Electroactuation of fluid using topographical wetting transitions," Langmuir **21**, 12218 (2005).
[19]J. Melcher and G. Taylor, "Electrohydrodynamics: a review of the role of interfacial shear stresses," Annu. Rev. Fluid Mech. **1**, 111 (1969).